An X- and Ku-band multifunctional radar receiver based on photonic parametric sampling

Lei Yu (于 磊), Weiwen Zou (邹卫文)*, Xinwan Li (李新碗), and Jianping Chen (陈建平)

State Key Laboratory of Advanced Optical Communication Systems and Networks, Intelligent Microwave Lightwave Integration Innovation Center (iMLic), Shanghai Institute for Advanced Communication and Data Science, Department of Electronic Engineering, Shanghai Jiao Tong University, Shanghai 200240, China

**Corresponding author: wzou@sjtu.edu.cn*

Received September 15, 2019; accepted December 26, 2019; posted online April 7, 2020

We demonstrate a novel multifunctional radar receiver scheme based on photonic parametric sampling. The working principle of photonic parametric sampling based on four-wave mixing (FWM) process is presented. To experimentally verify the multifunctional feasibility, the scheme is individually implemented to carry out a four-channel phased array radar reception and a dual-band radar reception.

Keywords: microwave photonics; radar receiver; photonic parametric sampling; four-wave mixing.
doi: 10.3788/COL202018.042501.

With the demand for radar's ubiquitous applicability, many advanced technologies have been developed[1,2]. However, the slowdown of electronic technology introduces new challenges for both hardware design and digital signal processing. Due to the broadband nature, immunity to electromagnetic interference, and system reconfigurability, microwave photonics or photonics-assisted radio-frequency (RF) technology has become a very attractive candidate for broadband signal processing applications[3]. Different kinds of photonics-based radar schemes have been recently proposed[3–13], among which lots of effort has been devoted to developing the photonic generation/transmission of radar RF signals[4,5] and photonic reception/processing of radar echoes[6–13]. In Ref. [4], a photonic transceiver was incorporated into a coherent radar architecture and it was tested in a field-trial demonstration. However, multiple functions integrated in one architecture are essentially required to take advantage of the broadband nature of microwave photonics. A photonics-based dual-functional system is proposed for radar imaging and frequency measurement[14], which proves the ability to process multiple signals.

Another trend of radar development is the demand for high-speed signal processing. Photonic analog-to-digital conversions (ADCs)[15] have shown significant improvements in terms of sampling speed and sampling resolution for the direct reception of radar RF signals. However, its sampling gate based on a Mach–Zehnder modulator (MZM) is limited by the modulation bandwidth[16–20]. For a photonics-based radar system, the cascade of photonic signal processing (e.g., photonic beamforming) and MZM-based photonic sampling will induce extra electrical-to-optical (E/O) and optical-to-electrical (O/E) conversion. To avoid the optical-to-electrical-to-optical (OEO) conversion and promote an all-optical signal processing in a radar system, the photonic parametric sampling based on a nonlinear effect of the four-wave mixing (FWM) process is demonstrated. In this scheme, an optical pulse train is used as the pump beam (ω_2) and parametrically mixed with a signal beam (ω_1), which interacts along the nonlinear waveguide to generate the converted copy (ω_3)[21–23]. This parametric mixing process can be used as the all-optical sampling, allowing the sampled signal to be either optical or RF-originated (i.e., RF imprinted on an optical signal).

In this Letter, we propose a multifunctional radar receiver scheme via FWM-based photonic parametric sampling. The FWM process is applied to realize the parallel configuration of the radar receiver scheme. After demonstration of the working principle, a four-channel phased array radar reception and a dual-band radar reception are implemented in experiments. The proposed radar receiver scheme can achieve an integration of the parallel signal processing for a multifunctional radar receiver and high-speed signal processing, potentially improving the performance of a photonics-based radar system.

The working principle of the multifunctional radar receiver scheme via FWM-based photonic signal processing is illustrated in Fig. 1. Optical signals at different

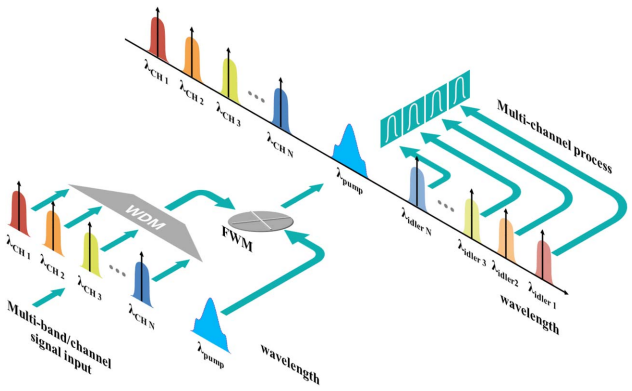

Fig. 1. Working principle of multifunctional radar receiver scheme for parallel signal processing based on the FWM process.

wavelengths ($\lambda_{\mathrm{CH1}}, \lambda_{\mathrm{CH2}}, \ldots, \lambda_{CHN}$) serve as the multichannel light sources and are combined by a wavelength division multiplexer (WDM) into one beam. After being modulated by the RF signals to be processed, the beam is injected into a nonlinear processing element and another optical pulse source (λ_{pump}) is used as the pump signal of the FWM process. In the nonlinear processing element, each optical signal of the multichannel light sources is parametrically mixed with the pump signal through the FWM process for the photonic parametric sampling, generating N idlers ($\lambda_{\mathrm{idler1}}, \lambda_{\mathrm{idler2}}, \ldots, \lambda_{\mathrm{idler}N}$). Each idler is filtered out optically and processed in parallel, which can be equivalent to N radar receivers. Thus, the FWM-based photonic parametric sampling can be programmed for different functionality by the same multichannel light source.

Figure 2 depicts the proof-of-concept experimental setup for the proposed multifunctional radar receiver scheme based on photonic parametric sampling. A four-channel tunable laser (Alnair Labs TLG-200) is used as the multichannel light sources and the wavelengths of four channels are set to be $\lambda_1 = 1542.1$ nm, $\lambda_2 = 1543.8$ nm, $\lambda_3 = 1545.3$ nm, and $\lambda_4 = 1546.9$ nm, respectively. Each channel is connected to a Mach–Zehnder modulator (MZM, Photline MXAN-LN-40) that serves as the electrical-optical conversion for modulation of the RF signal to be processed. The multiplexed optical signal by a WDM is connected to the first port of a circulator, and the second WDM connected with four one-port variable optical delay lines (VODLs, General Photonics MDL-002) serves as the time delay adjuster of each channel. The time-adjusted optical signals are reflected back to the second port of the circulator through the second WDM. The power of the optical signal from the third port of the circulator is amplified by an erbium-doped fiber amplifier (EDFA, Calmar AMP-ST 18).

An actively mode-locked laser (AMLL, Calmar PSL-10-TT) is locked to a 10 GHz reference generated from a microwave synthesizer (Keysight E8257D). The optical output from the AMLL is amplified by another EDFA (Calmar AMP-ST 30), which serves as the pump signal of the FWM-based photonic parametric sampling. The pump signal and multiplexed multichannel light sources are combined by an optical coupler (OC) and injected into a 9 m long photonic crystal fiber (PCF) with a nonlinear coefficient of ~11 rad $\cdot$ W^{-1} $\cdot$ km^{-1} at 1550 nm (NKT Photonics NL-1550-POS-1-100409)[24]. The idlers at different wavelengths are optimized in amplitude by controlling the polarization states of the pump signal and multiplexed multichannel light sources. The idlers are filtered out by an optical band pass filter (OBPF, Alniar Labs CVF-220CL) and converted into an electrical signal by the photodetector (PD, Conquer PDA-10 G-InGaAs-SM-FA), which are digitized by an oscilloscope (OSC, Keysight MSOS804A).

Since the FWM-based photonic parametric sampling generates the idlers at different wavelengths, the FWM wavelength conversion efficiency (η_t) or optical power uniformity of the idlers generated by different-channel signals determines the amplitude of the converted electrical signal, which affects the parallel signal processing explained afterward. η_t can be expressed by

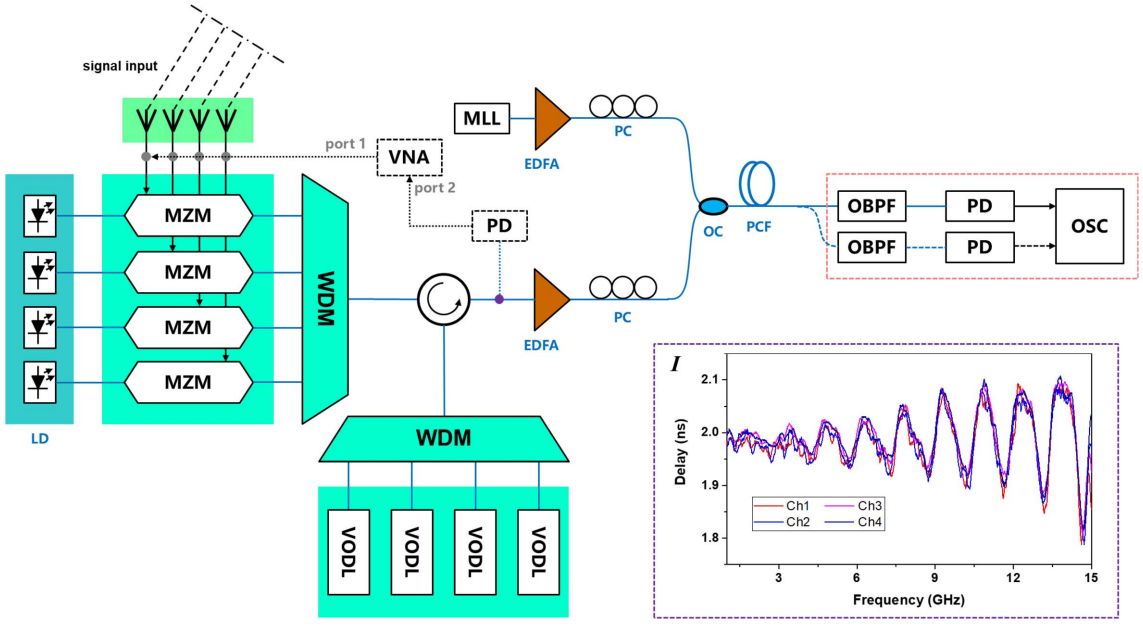

Fig. 2. Experimental setup for multi-functional radar receiver based on photonic parametric sampling. LD: laser diode, MZM: Mach–Zehnder modulator, WDM: wavelength division multiplexer, VODL: variable optical delay line, EDFA: erbium-doped fiber amplifier, PC: polarization controller, MLL: mode-locked laser, OC: optical coupler, PCF: photonic crystal fiber, OBPF: optical band pass filter, PD: photodetector, OSC: oscilloscope, VNA: vector network analyzer. Inset I indicates the matched time delay of four channels.

$$\eta_t = 10\log\left(\frac{P_i}{P_s}\right), \tag{1}$$

where P_s is the power of the light source in the nth channel and P_i is the power of the idler optical signal generated by the light source and pump signal. In the experiment, η_t in the PCF is measured as the function of the wavelength of the light source and the pump signal is fixed at 1560 nm, which is illustrated in Fig. 3. The fluctuation within the wavelength range of the four-channel light source (in the dashed box of Fig. 3) is about 1.3 dB.

In order to verify the feasibility of multifunctional radar signal reception, two individual experiments are carried out based on the same setup as in Fig. 2. First, we testify the ability of the four-channel phased array radar reception. As shown in Fig. 2, the four channels of the tunable laser are all turned on to form the multichannel light sources. By adjusting the optical powers of light sources, the optical-link power for each channel can be optimized separately. Port 1 of a vector network analyzer (VNA, Agilent PNA-X Network Analyzer N5247A) is connected to the RF input port of the four MZMs. Port 2 of the VNA is connected with the PD laid behind the third port of the circulator. As depicted in the inset I of Fig. 2, the time delays of four channels for the phased array radar receiver are matched by adjusting the VODLs. Another microwave generator (Keysight MXG N5183B) is used to generate the RF signal, which is divided into four parts by a power splitter. Each part is connected to an MZM for RF reception. The combined optical signals of four channels are parametrically sampled through the PCF. The optical spectra of the photonic parametric sampling of the four-channel RF signals are compared in Fig. 4. The idlers are filtered out by the OBPF and the converted electrical signal is digitized by the OSC. The time delays of four modulated multichannel light sources are set as an arithmetic sequence. The time delay difference ($\delta\tau$) of the four channels is set to be swept at a step of 5 ps. Figure 5 illustrates the beam-forming pattern of the four-channel phased array radar receiver at the X band, where the

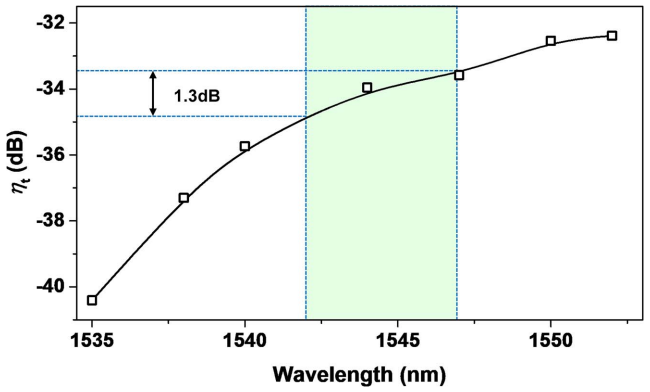

Fig. 3. FWM wavelength conversion efficiency at different wavelengths when the wavelength of the pump signal is fixed at 1560 nm.

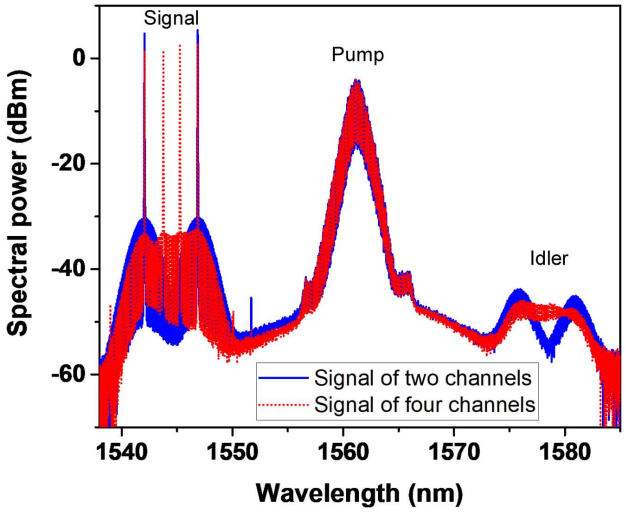

Fig. 4. Optical spectra of the photonic parametric sampling in the PCF for different-channel signals.

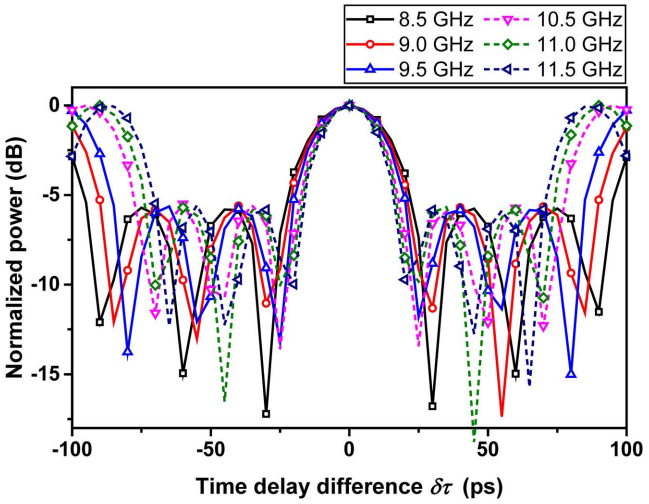

Fig. 5. Measured (symbols) and simulated (curves) beam-forming pattern of the four-channel phased array radar reception operating at the X band.

vertical axis is normalized to the maximum values of the curves. As shown in Fig. 5, the main lobe can be detected with the time delay sweeping of the optical delay lines[25]. The linewidth of the main lobe is apparently decreased with the increase of the RF signal's frequency.

According to the principle of phased array radar technology, the RF signal is coupled to the radar antennas at different times, generating phase differences among the signals at the output of the antennas (i.e., the signals directly modulated to the MZMs in this study). The phase difference can be expressed by

$$\Delta_\varphi = \left(2\pi d/\lambda_{\mathrm{RF}}\right)\sin\theta, \tag{2}$$

where d is the spatial distance between the neighboring antennas, λ_{RF} is the wavelength of the received RF signal,

and θ is the scanning angle. The neighboring channels introduce an extra phase difference that is described by

$$\Delta_B = 2\pi f_{\mathrm{RF}} \delta\tau, \tag{3}$$

where $f_{\mathrm{RF}} = c/\lambda_{\mathrm{RF}}$ is the frequency of the received RF signal, with c being the light speed in vacuum, and $\delta\tau$ is the time delay difference among the neighboring channels.

For a uniformly-distributed phased array radar receiver, the amplitude pattern can be given by[25]

$$|F(\delta\tau)| = \frac{\sin\{N[(2\pi d/\lambda_{\mathrm{RF}})\sin\theta - 2\pi f_{\mathrm{RF}}\delta\tau]/2\}}{\sin\{[(2\pi d/\lambda_{\mathrm{RF}})\sin\theta - 2\pi f_{\mathrm{RF}}\delta\tau]/2\}}, \tag{4}$$

where N is the number of channels. The scanning angle θ and the number of channels N are set to be 0 and 4, respectively. The numerical simulation based on Eq. (4) is also plotted in Fig. 5 and it agrees well with the experiment results.

Another experiment of the multifunctional scheme for dual-band radar reception is further carried out based on the same setup as in Fig. 2. Only two channels of the tunable laser (Ch 1 and Ch 4) are turned on, and the time-delay adjustment is not necessary. Two microwave generators (Keysight MXG N5183B and Rhode & Schwarz SMA 100A) are used to generate dual-band RF signals, which are modulated to two MZMs in the two channels. The two-channel modulated signals are parametrically sampled by the pump signal in the PCF and the corresponding spectrum is also illustrated in Fig. 4. The two idlers do not interact with each other in frequency, which can be easily separated by the OBPFs and detected by the two PDs. The electrical signals converted by the PDs are processed in parallel by the OSC. Note that the sampling rate of the OSC is set to 10 GSa/s for each channel. In this scheme, two channel signals can be received at the same time.

X band (at 11 GHz) and Ku band (at 17 GHz) signals are simultaneously injected into the receiver, and the experimental result is depicted in Fig. 6. Due to the repetition rate of the pump signal and the sampling theory, the signal frequencies of 11 GHz and 17 GHz are aliased to 1 GHz and 3 GHz in the Nyquist band, respectively. The experimental result shows the feasibility of the multifunctional scheme for the dual-band radar reception. As a proof-of-concept experiment, the sampling rate of the system in this work is set to be 10 GSa/s, which indicates that the operating instantaneous bandwidth can reach 5 GHz. Because the EDFAs are used in the experimental setup and the FWM conversion efficiency in the PCF is relatively low, the signal-to-noise ratio (SNR) should be optimized in the future by use of other nonlinear elements with high nonlinear coefficients.

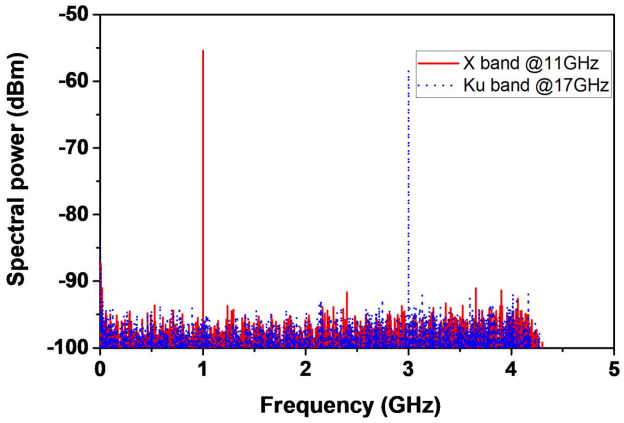

Fig. 6. Electric spectra of two received signals at X band and Ku band with 10 GSa/s sampling rate.

We have demonstrated a multifunctional radar receiver scheme via FWM-based photonic parametric sampling in a 9 m long PCF, leading to the achievement of parallel signal processing in a unique setup. A four-channel phased array radar reception at the X band and a dual-band radar reception at the X and Ku bands are experimentally carried out by use of the same scheme. Since the multichannel sampling process can be realized in one parametric sampling gate, the radar system can be simplified. Thanks to the ultra-broad bandwidth of the photonic parametric sampling, the scheme is expected to play an important role in the next-generation photonics-based radar system with multiple functions.

This work was supported in part by the National Natural Science Foundation of China (Nos. 61822508, 61571292, and 61535006).

References

1. A. Hassanien and S. A. Vorobyov, IEEE Trans. Signal Process. **58**, 3137 (2010).
2. M. I. Skolnik, *Introduction to Radar Systems* (McGraw-Hill, 2001).
3. J. Yao, J. Lightwave Technol. **27**, 314 (2009).
4. P. Ghelfi, F. Laghezza, F. Scotti, G. Serafino, A. Capria, S. Pinna, D. Onori, C. Porzi, M. Scaffardi, A. Malacarne, V. Vercesi, E. Lazzeri, and A. Bogoni, Nature **507**, 341 (2014).
5. W. Zou, H. Zhang, X. Long, S. Zhang, Y. Cui, and J. Chen, Sci. Rep. **6**, 19786 (2016).
6. H. Emami, N. Sarkhosh, and M. Ashourian, Opt. Express **21**, 7734 (2013).
7. F. Zhang, B. Gao, and S. Pan, Opt. Express **26**, 17529 (2018).
8. F. Zhang, Q. Guo, and S. Pan, Sci. Rep. **7**, 13848 (2017).
9. N. Shi, M. Li, Y. Deng, L. Zhang, S. Sun, J. Tang, W. Li, and N. Zhu, Opt. Express **24**, 14438 (2016).
10. X. Ye, B. Zhang, Y. Zhang, D. Zhu, and S. Pan, Chin. Opt. Lett. **15**, 010013 (2017).
11. S. Xu, W. Zou, G. Yang, and J. Chen, Chin. Opt. Lett. **16**, 062801 (2018).
12. Z. Meng, J. Li, C. Yin, Y. Fan, F. Yin, Y. Zhou, Y. Dai, and K. Xu, Opt. Express **25**, 22055 (2017).
13. G. Yang, W. Zou, Y. Yuan, and J. Chen, Chin. Opt. Lett. **16**, 030601 (2018).
14. J. Shi, F. Zhang, X. Ye, Y. Yang, D. Ben, and S. Pan, Opt. Lett. **44**, 1948 (2019).
15. G. C. Valley, Opt. Express **15**, 1955 (2007).
16. H. Zhang, W. Zou, G. Yang, and J. Chen, Chin. Opt. Lett. **14**, 030602 (2016).

17. G. Yang, W. Zou, L. Yu, and J. Chen, Opt. Lett. **43**, 3530 (2018).
18. S. Xu, X. Zou, B. Ma, J. Chen, L. Yu, and W. Zou, Light Sci. Appl. **8**, 66 (2019).
19. L. Yu, W. Zou, G. Yang, W. Li, and J. Chen, Chin. Opt. Lett. **16**, 120602 (2018).
20. F. Yang, W. Zou, L. Yu, S. Xu, and J. Chen, Chin. Opt. Lett. **17**, 040602 (2019).
21. D. Jafari, T. Nurmohammadi, M. J. Asadi, and K. Abbasian, Opt. Laser Technol. **101**, 138 (2018).
22. D. J. Esman, A. O. J. Wiberg, M. H. Yang, L. Liu, B. P. P. Kuo, N. Alic, and S. Radic, in *European Conference on Optical Communication* (2014), p. 1.
23. S. Radic, IEEE J. Sel. Top. Quantum Electron. **18**, 670 (2012).
24. B. Ma, L. Yu, J. Chen, and W. Zou, IEEE Photonics Technol. Lett. **31**, 595 (2019).
25. A. Yu, W. Zou, S. Li, and J. Chen, IEEE Photonics J. **6**, 7902310 (2014).